Egypt. J. Chem. Vol. **68**, No.2, pp. 183 - 192 (2025)

Egyptian Journal of Chemistry

http://ejchem.journals.ekb.eg/

Synthesis, Characterization and Glyoxalase Inhibitory Activity of 4,6-Diheteroarylpyrimidine-2-amine Derivatives: *In Vitro* and *In Silico* Studies

Mohammad Murwih Alidmat [1,2], Maram B. Alhawarri [2], Mahmoud Al-Refai [1], Iman A. Mansi [3], Qosay Al-Balas [4], and Mohammad M. Ibrahim [1*]

[1] *Department of Chemistry, Faculty of Science, Al al-Bayt University, P.O.BOX 130040, Al-Mafraq 25113, Jordan.*
[2] *Department of Pharmacy, Faculty of Pharmacy, Jadara University, P.O.Box 733, Irbid 21110, Jordan.*
[3] *Department of Clinical Pharmacy and Pharmacy Practice, Faculty of Pharmaceutical sciences, The Hashemite University, Zarqa, Jordan.*
[4] *Department of Medicinal Chemistry and Pharmacognosy, Faculty of Pharmacy, Jordan University of Science and Technology, Irbid, Jordan.*

Abstract

New series of 4,6-diheteroarylpyrimidine-2-amines (**4a-e**) and (**5a-c**) were prepared by cyclization of particular chalcones (**2**) or (**3**) with guanidine nitrate in the presence of potassium hydroxide. Chalcones (**2**) and (**3**) were prepared by base-catalyzed Claisen-Schmidt condensation of heteroaryl aldehydes (**1**) with 2-acetyl-5-chlorothiophene and 3-acetyl-2,5-dichlorothiophene, respectively. All the newly synthesized compounds were characterized by spectroscopic and spectrometric techniques such as IR, ^{1}H NMR, ^{13}C NMR and mass spectrometry. This study evaluated *in vitro* glyoxalase I (GLO-I) inhibitory activity, coupled with molecular docking analysis. Spectroscopic methods confirmed the structures, and structure-activity relationship was established, revealing the importance of chloro substitutions and a furan ring for enhanced inhibition. *In vitro* glyoxalase inhibitory activity showed that **5b** has excellent inhibitory activity against the glyoxalase I enzyme, with an IC_{50} of 15 µM. Molecular docking using AutoDock 4.2 highlighted key interactions within the active site of the human glyoxalase I enzyme, underscoring the absence of direct Zn interactions in the synthesized compounds compared to the cocrystallized ligand and revealing the need for structural optimization to introduce metal-binding functionalities. This research paves the way for the rational design of more potent glyoxalase I inhibitors, contributing significantly to the field of enzyme inhibition and therapeutic agent development.

*Keywords***:** Pyrimidines; Glyoxalase-I; Molecular Docking

1. Introduction

Methylglyoxal (MG), a highly reactive dicarbonyl compound formed as a byproduct of glycolysis, has emerged as a critical factor in the pathogenesis of various diseases [1, 2]. Elevated levels of MG are implicated in the formation of advanced glycation end products (AGEs), oxidative stress, and cellular damage, contributing to the progression of conditions such as diabetes, neurodegenerative disorders, and cancer [3]. The glyoxalase system, which includes glyoxalase I (GLO-I) and glyoxalase II (GLO-II), serves as a crucial defense mechanism against the cytotoxic effects of MG and other reactive metabolites [4]. GLO-I catalyses the conversion of harmful MG to non-toxic D-lactate, thereby preventing the deleterious consequences associated with MG-induced protein modifications and AGE formation [5]. Overexpression of GLO-I in cancerous cells has prompted researchers to identify potent GLO-I inhibitors as a promising strategy for sensitizing cancer cells to treatment [4].
Recent research has concentrated on identifying potent inhibitors of the glyoxalase I (GLO-I) enzyme, recognized for its potential in anticancer therapy [6]. This effort has led to the discovery of various inhibitors with activities ranging from high micromolar to low nanomolar IC_{50} or Ki values [7, 8]. Among these, compounds revealed through high-throughput screening and fragment-based drug discovery techniques have emerged as particularly promising. However, despite the exploration of a wide array of chemotypes and the employment of sophisticated methods such as pharmacophore modelling, the clinical application of GLO-I inhibitors remains unexplored [7, 9, 10]. This gap highlights the critical need for ongoing innovation in the development of strategies aimed at the effective targeting of GLO-I in cancer treatment.

In this context, pyrimidine derivatives have demonstrated remarkable potential as anticancer agents, offering a versatile scaffold for the design and synthesis of novel glyoxalase I inhibitors, especially pyridine-based chalcone derivatives [11-15]. Previous study have highlighted the inhibitory activity of pyrimidine derivatives against GLO-I, underscoring their relevance in modulating the glyoxalase system [16]. By leveraging the insights from this study, the investigation of pyrimidine derivatives

*Corresponding author e-mail: mohammadibrahim@aabu.edu.jo.;(Mohammad M. Ibrahim)
Receive Date: 16 May 2024, Revise Date: 18 June 2024, Accept Date: 02 July 2024,
DOI: 10.21608/ejchem.2024.289371.9720

as GLO-I inhibitors represents a compelling avenue for drug discovery. Furthermore, the study of the interactions of pyrimidine derivatives with the active site of GLO-I presents an opportunity to elucidate the structure-activity relationships governing enzyme inhibition, facilitating the rational design of potent and selective inhibitors.

This research article aims to design, synthesize, and biologically evaluate pyrimidine derivatives as glyoxalase I inhibitors, followed by molecular docking analysis to elucidate the binding interactions and inhibitory mechanisms of pyrimidine derivatives with GLO-I. By elucidating these mechanisms, we aspire to contribute to the development of a comprehensive overview of the conditions that necessitate the inhibition of GLO-I for the identification of novel therapeutic agents for diseases associated with glyoxalase dysregulation, such as cancer.

2. Materials and Methods

All chemicals used in this work were purchased from Aldrich or Acros and were of analytical grade or higher.

2.1. Instrumentation

Melting points were determined using an Electrothermal-9100 melting point apparatus. For infrared (IR) spectroscopy, KBr discs were analysed on a Nicolet Impact-400 FT-IR spectrometer. ^{1}H and ^{13}C NMR spectra were recorded at room temperature using a Bruker 300 MHz ultrashield spectrometer. DMSO-*d*$_6$ was used as the NMR solvent, and chemical shifts are expressed in ppm with reference to TMS as an internal standard. The purity of the compounds was verified using elemental analysis. Elemental compositions were determined on a Euro-vector EA 3000A analyser. These analyses were carried out at the Central Laboratories of Al al-Bayt University in Mafraq, Jordan. Mass spectrometric analyses were performed on an API 3200 Q-TRAP spectrometer (+ve ESI, product ion scan, MS2, 35 eV) at the Jordan University of Science and Technology. Chalcones (**2a-e**) and (**3a-c**) were prepared according to the literature procedures [17, 18]. Biological activity evaluations were conducted at the Department of Medicinal Chemistry and Pharmacognosy, Faculty of Pharmacy, Jordan University of Science and Technology, Irbid, Jordan.

2.2. Compounds Synthesis

*2.2.1. General procedures for the preparation of 4,6-diheteroarylpyrimidine-2-amines **4a-e** and **5a-c** [19].*

A mixture of chalcone **2** or **3** (0.01 mol) and guanidine nitrate (0.01 mol, 1.0 equiv.) was stirred in ethanol (25 mL) at room temperature [20]. Potassium hydroxide (0.011 mol) was then added gradually. The reaction mixture was refluxed with stirring for 24 h. The progress of the reaction was monitored by TLC. After completion of the reaction, the reaction mixture was poured into ice water to give a precipitated solid, which was filtered off, washed with diethyl ether (2 × 30 mL) and then dried. The obtained solid was recrystallized from ethanol to form the desired pyrimidine-2-amine derivatives.

*4-(5-Chlorothiophen-2-yl)-6-(thiophen-2-yl)pyrimidin-2-amine (**4a**)*

Yellow precipitate; 67% yield; m.p 147-150°C dec. IR (KBr, cm^{-1}): ν = 3485 (br, NH_2), 2413 (C-H), 1554 (C=N). ^{1}H NMR (300 MHz, DMSO-*d6*): δ (ppm) = 8.34 (d, *J* = 4.2 Hz, 1H, H-3"), 8.12 (s, 1H, H-5), 7.75 (d, *J* = 3.9 Hz, 1H, H-3'), 7.21 (d, *J* = 3.7 Hz, 1H, H-5"), 7.08 (t, *J* = 4.1 Hz, 1H, H-4"), 7.07 (d, *J* = 3.8 Hz, 1H, H-4'), 6.61 (s, 2H, NH_2). ^{13}C NMR (75 MHz, DMSO-*d6*, ppm) δ: (C-NH_2: 163.2), (C=N: 159.9), (C-4: 158.7), 142.8, 142.1, 130.0, 129.9, 128.9, 128.3,127.5, 126.8, (C-5: 98.0). ESIMS: m/z 294.3 [M+H].

*4-(5-Chlorothiophen-2-yl)-6-(furan-2-yl)pyrimidin-2-amine (**4b**)*

Yellow precipitate; 62% yield; m.p 171-173°C dec. IR (KBr, cm^{-1}): ν = 3650 (br, NH_2), 2390 (C-H), 1469 (C=N). ^{1}H NMR (300 MHz, DMSO-*d6*): δ (ppm) = 8.07 (s, 1H, H-5), 7.85 - 6.92 (m, 5 H, H-3', H-4', H-3", H-4", and H-5"), 6.88 (s, 2H, NH_2). ^{13}C NMR (75 MHz, DMSO-*d6*, ppm) δ: (C-NH_2: 163.3), (C=N: 159.5), (C-4: 158.9), 158.3, 145.3, 141.9 132.1, 128.3, 127.5, 112.4, 111.8, (C-5: 97.7). ESIMS: m/z 278.1 [M+H].

*4-(5-Chlorothiophen-2-yl)-6-(1H-pyrrol-2-yl)pyrimidin-2-amine (**4c**)*

Brown precipitate; 61% yield; m.p 97-100°C dec. IR (KBr, cm^{-1}): ν = 3475 br, NH, NH_2), 2329 (C-H), 1532 (C=N). ^{1}H NMR (300 MHz, DMSO-*d6*): δ (ppm) = 11.85 (s, 1H, NH), 8.01 (s, 1H, H-5), 7.81 (d, *J* = 3.8 Hz, 1H, H-3'), 7.41 (d, *J* = 3.9 Hz, 1H, H-4'), 7.06 (d, *J* = 3.6 Hz, 1H, H-5"), 6.78 (d, *J* = 3.8 Hz, 1H, H-3"), 6.29 (t, *J* = 3.5 Hz, 1H, H-4"), 6.87 (s, 2H, NH_2). ^{13}C NMR (75 MHz, DMSO-*d6*, ppm) δ: (C-NH_2: 166.5), (C=N: 163.5), (C-4: 158.9), 145.3, 133.8, 131.5, 128.9, 124.6, 116.4, 113.4, 110.8, (C-5: 97.4). ESIMS: m/z 278.1 [M+2].

*4-(4-Bromothiophen-2-yl)-6-(5-chlorothiophen-2-yl)pyrimidin-2-amine (**4d**)*

Yellow precipitate; 78% yield; m.p 121-124°C dec. IR (KBr, cm^{-1}): ν = 3470 (br, NH_2), 2408 (C-H), 1549 (C=N). ^{1}H NMR (300 MHz, DMSO-*d6*): δ (ppm) = 8.11 (s, 1H, H-5), 7.94 (d, *J* = 3.9 Hz, 1H, H-3'), 7.87 (s, 1H, H-3"), 7.75 (s, 1H, H-5"), 7.28 (d, *J* = 3.9 Hz, 1H, H-4'), 6.87 (s, 2H, NH_2). ^{13}C NMR (75 MHz, DMSO-*d6*, ppm) δ: : (C-NH_2: 163.2), (C=N: 159.2), (C-4: 158.4), 144.1, 141.8, 133.7, 129.8, 128.4, 127.8, 127.5, 109.6, , (C-5: 98.1).. ESIMS: m/z 374.2 [M+2].

*4-(5-Chlorothiophen-2-yl)-6-(furan-3-yl)pyrimidin-2-amine (**4e**)*

Yellow precipitate; 78% yield; m.p 121-124°C dec. IR (KBr, cm^{-1}): ν = 3480 (br, NH_2), 2405 (C-H), 1559 (C=N). ^{1}H NMR (300 MHz, DMSO-*d6*): δ (ppm) = 8.05 (s, 1H, H-5), 7.78 (d, *J* = 4.0 Hz, 1H, H-3'), 7.74 (s, 1H, H-2"), 7.33 (d, *J* = 3.2 Hz, 1H, H-5"), 7.26 (d, *J* = 4.1 Hz, 1H, H-4'), 7.15 (d, *J* = 3.0 Hz, 1H, H-4"), 6.87 (s, 2H, NH_2). ^{13}C NMR (75 MHz, DMSO-*d6*, ppm)

δ: (C-NH_2: 163.4), (C=N:159.5), (C-4: 158.7), 144.8, 141.8, 132.3, 128.9, 128.2, 127.5, 127.35, 111.6, (C-5: 97.8). ESIMS: m/z 278.1 [M+H].

4-(2,5-Dichlorothiophen-3-yl)-6-(thiophen-2-yl)pyrimidin-2-amine ***(5a)***
Yellow solid. 81% yield. m.p: 173-176°C dec. IR (KBr, cm^{-1}): ν = 3480 (br, NH_2), 1331 (C-H), 1565 (C=N). ^{1}H NMR (300 MHz, DMSO-*d6*): δ (ppm) = 7.98 (s, 1H, H-5), 7.82 (d, *J* = 3.5, 1H, H-3"), 7.58 (d, *J* = 4.2 Hz, 1H, H-5"), 7.48 (s, 1H, H-4'), 7.23 (t, *J* = 5.0 Hz, 1H, H-4"), 6.84 (s, 2H, NH_2). ^{13}C NMR (75 MHz, DMSO-*d6*, ppm) δ: (C-NH_2: 163.5), (C=N: 160.1), (C-4: 158.9), 143.3, 142.6, 136.12, 130.2, 128.4, 128.03, 127.9, 125.2, (C-5: 102.5). ESIMS: m/z 328.3 [M^+].

4-(2,5-Dichlorothiophen-3-yl)-6-(furan-3-yl)pyrimidin-2-amine ***(5b)***
Brown solid. 84% yield. m.p: 153-157°C dec. IR (KBr, cm^{-1}): ν = 3420 (NH_2), 2345 (C-H), 1635 (C=N). ^{1}H NMR (300 MHz, DMSO-*d6*): δ (ppm) = 8.43 (s, 1H, H-5), 7.88 (s, 1H, H-2"), 7.55 (s, 1H, H-4'), 7.31 (d, *J* = 2.9 Hz, 1H, H-5"), 7.10 (d, *J* = 3.8 Hz, 1H, H-4"), 6.76 (s, 2H, NH_2). ^{13}C NMR (75 MHz, DMSO-*d6*, ppm) δ: (C-NH_2: 163.6), (C=N: 159.9), (C-4:158.8), 143.8, 143.6, 136.1, 127.9, 125.6, 125.2, 125.1, 108.5, (C-5: 104.2). ESIMS: m/z 313.2 [M+H].

4-(2,5-dichlorothiophen-3-yl)-6-(1H-pyrrol-2-yl)pyrimidin-2-amine ***(5c)***
Yellow solid. 86% yield. mp: 164-166°C dec. IR (KBr, cm^{-1}): ν = 3730 (NH_2), 2450 (C-H), 1620 (C=N). ^{1}H NMR (300 MHz, DMSO-*d6*): δ (ppm) = 8.09 (s, 1H, H-5), 7.90 (s, 1H, H-3"), 7.57 (s, 1H, H-5"), 7.53 (s, 1H, H-4'), 6.90 (s, 2H, NH_2). ^{13}C NMR (75 MHz, DMSO-*d6*, ppm) δ: (C-NH_2: 163.7), (C=N: 163.2), (C-4: 159.1), 139.2, 136.1, 133.3, 130.9, 129.4, 128.1, 125.9, 122.2, (C-5: 104.2). ESIMS: m/z 408.1 [M+H].

2.3. Glyoxalase Inhibitory Activity Assay

The glyoxalase inhibitory activity of the synthesized compounds was evaluated through a colorimetric assay [21, 22]. The enzyme glyoxalase I (GLO-I), derived from *E. coli* (Ala2-Met184, N-terminal Met, 6-His tag), was obtained from R&D. The enzymatic activity was determined based on its capacity to catalyze the formation of S-D-lactoylglutathione from methylglyoxal (MG) and reduced glutathione (GSH).
Initially, 100 mM GSH and 100 mM MG were freshly prepared using deionized water. The substrate mixture for the assay was constituted by combining 1420 µL of 0.1 M assay buffer (phosphate monobasic and phosphate dibasic) with a pH of 7.2, 40 µL of freshly prepared 100 mM GSH, and 40 µL of 100 mM methylglyoxal, followed by a 15-minute incubation at room temperature. Subsequently, recombinant human glyoxalase I (rhGlyoxalase I) was diluted to a concentration of 0.4 ng/µL using assay buffer. For the reaction, 2, 250 ml of assay buffer, 750 µl of substrate solution, 15 µl of the inhibitor at varying concentrations (0.002 mM to 10 mM) and 1.3 µl of the enzyme solution (GLO-I) were loaded into a cuvette with a final volume of 3 ml. A control sample consisting of 750 µL of enzyme assay buffer, 2,250 µL of substrate mixture, and 15 µL of dimethyl sulfoxide (DMSO) was also prepared. The reaction mixture was incubated for 15 minutes at room temperature. The absorbance was measured with a UV-Spectrometer (Spectroscan 60 DV) at a λ_{max} of 240 nm over a 5-minute period in kinetic mode, with a 5-second mixing period before the first reading and a 3-second mixing period between subsequent readings.
The percent inhibition was calculated for each compound at the highest tested concentration (10 mM). Afterward, the IC_{50} values for compounds showing 75% or greater inhibitory activity were determined using serial dilutions of 5 mM, 2 mM, 1 mM, 0.2 mM, 0.02 mM, and 0.002 mM, and all experiments were conducted in triplicate to ensure the reliability of the findings. To assess the statistical significance of differences in glyoxalase I inhibitory activities among our series of synthesized compounds, we employed one-way analysis of variance (ANOVA) using Prism software (GraphPad Software, San Diego, CA, USA).

2.4. Molecular Docking Simulation
2.4.1 Protein preparation

The X-ray crystal structure of the human glyoxalase I enzyme (PDB ID: 3VW9) [23] was downloaded from the RCSB database [24]. All water molecules, including those within the active site, were removed using the Biovia Discovery Studio Visualizer [25-32]. Furthermore, heteroatoms were also removed [25-32]. The PDB2PQR web service [33] was utilized to conduct further calculations on the cleaned protein, which included reconstructing missing atoms and assigning atomic charges and radii, employing the SWANSON force field [26-28, 32]. The protonation states of the ionizable groups were determined using the empirical pKa predictor PROPKA3 [34], which was set to pH 7.4. Finally, the protonated enzyme was submitted to the MolProbity web service [35] to ensure the highest level of accuracy in the structural analysis and to correct contact atoms and add missing hydrogen atoms. This step was performed on December 15, 2023.

2.4.2 Ligand preparation

In this investigation, the compounds displaying the greatest inhibitory activity towards glyoxalase I were identified from Table 1 and sketched using PerkinElmer ChemDraw Professional 17.1 software (PerkinElmer, Massachusetts, USA) [26-31]. Specifically, compounds **5a**, **5b**, and **5c** exhibited the highest inhibitory activity (> 50%). The optimized geometries of these compounds were subsequently determined utilizing PerkinElmer Chem3D 17.1 and the Molecular Mechanics 2 force field (MM2) [36] and were saved in PDB format. To facilitate comparison, the cocrystallized ligand *N*-hydroxypyridone was extracted from the enzyme-ligand complex and saved as PDB files using the Biovia Discovery Studio Visualizer.
2.4.3 Docking and Scoring Protocol

Both the enzyme and ligands were prepared for docking using AutoDock Tools 1.5.6 [37], which is software developed by The Scripps Research Institute in La Jolla, CA, USA. The enzyme was assigned polar hydrogens and Kollman charges, while the ligands

were assigned Gasteiger charges and saved in PDBQT format. The docking parameters were set as follows: a grid box size of 40 × 40 × 40, a grid spacing of 0.375 Å, and coordinates of x = 8.86, y = -12.66, and z = -28.87 (centred on the active binding site), which were saved in grid parameter files (GPFs). In our simulations, the enzyme's structure was fixed in a rigid conformation to preserve the active site's stability and ensure the consistency of its structural integrity [38]. This rigidity contrasts with the treatment of ligands, which are flexible, enabling them to explore various conformations within the binding site [32, 39]. The docking procedure was executed through 100 runs of the Lamarckian genetic algorithm within AutoDock 4.2 [40]. This algorithm combines the principles of genetic algorithms with the effectiveness of local optimization techniques, a process termed 'Lamarckian' due to its incorporation of inherited traits (beneficial adaptations) into subsequent generations [41]. This methodology leverages AutoDock's advanced search capabilities, notably enhanced by its ΔG_{bind} correlation features derived from molecular conformations, to efficiently navigate the complex search space of possible ligand positions [41]. A population size of 150, a maximum of 2,500,000 evaluations (medium), and a maximum of 27,000 generations were chosen for the docking process. The remaining parameters were set to their default values and saved in docking parameter files (DPFs). AutoDock 4.2 was utilized to simulate the docking process, and the molecular interactions within the binding site were visualized and analysed using the BIOVIA Discovery Studio Visualizer.

3. Results and Discussion

3.1 Chemistry

3.1.1 Preparation of chalcones

Chalcones (**2a-e** and **3a-c**) were prepared by reacting aromatic aldehydes **(1)** with 2-acetyl-5-chlorothiophene or 3-acetyl-2,5-dichlorothiophene in a methanolic solution of potassium hydroxide at room temperature. Then, the 4,6-diheteroarylpyrimidine-2-amines **(4a-e** and **5a-c)** were prepared by refluxing the last chalcones **(2a-e** and **3a-c)** with guanidine nitrate in an ethanolic solution of potassium hydroxide for 24 hr. Pyrimidine-2-amine compounds **(4a-e** and **5a-c)** were obtained in very good yields, as shown in Scheme 1.

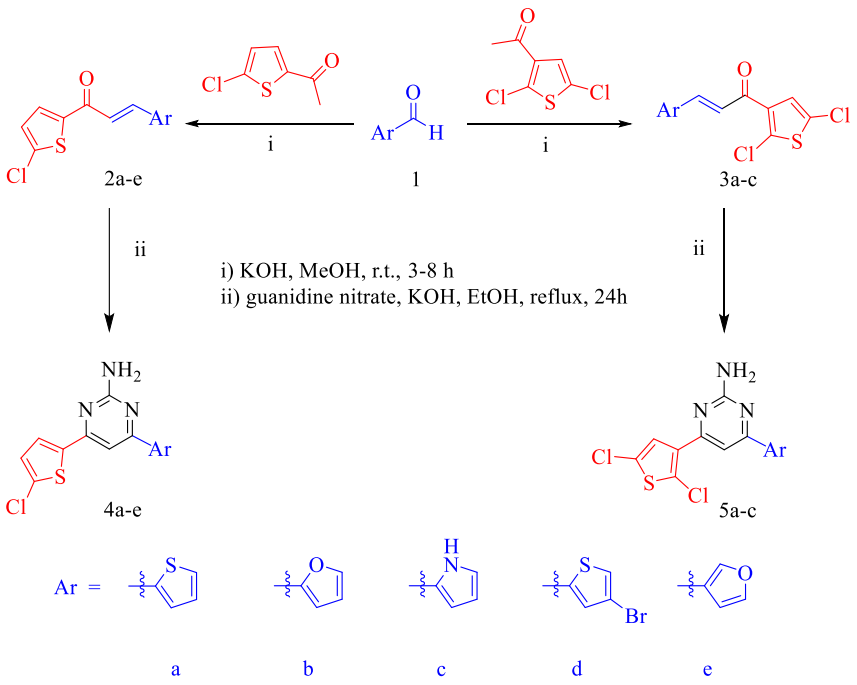

Scheme 1. Preparation of pyrimidine-2-amines containing thiophene.

The infrared spectra of pyrimidine-2-amines **(4a-e** and **5a-c)** showed a broad peak at 3420-3730 cm^{-1} attributed to NH_2 stretching vibrations. The peak at 1480-1650 cm^{-1} was attributed to the presence of C=N groups, and the peak at 1580-2435 cm^{-1} was attributed to C-H bond vibrations. The ^1H NMR (DMSO-*d6*) spectrum showed a singlet signal at *δ:* 7.16-8.11 ppm attributed to the proton of the pyrimidine ring. The protons of the NH_2 group appeared at *δ* 5.31-6.87 ppm, while the signals at 6.84–8.12 ppm were attributed to the protons of the heteroaromatic ring. The ^{13}C NMR (DMSO-*d6*) spectrum showed all carbon signals for the pyrimidine-2-amines **(4a-e** and **5a-c)**. The highly deshielded peaks at 158.6-163.2 ppm, 158.4-166.5 ppm, and 159.2-163.5 ppm were assigned to the quaternary carbons of the pyrimidine ring, while the peak at *δ* 97.4-104.2 ppm was assigned to

the C-5 atom of the pyrimidine ring. As an example, Figure 1 shows the ^{1}H NMR spectrum of compound **4c**. The MS spectra of the compounds display the correct molecular ion peaks, as suggested by the molecular formula [M+1].

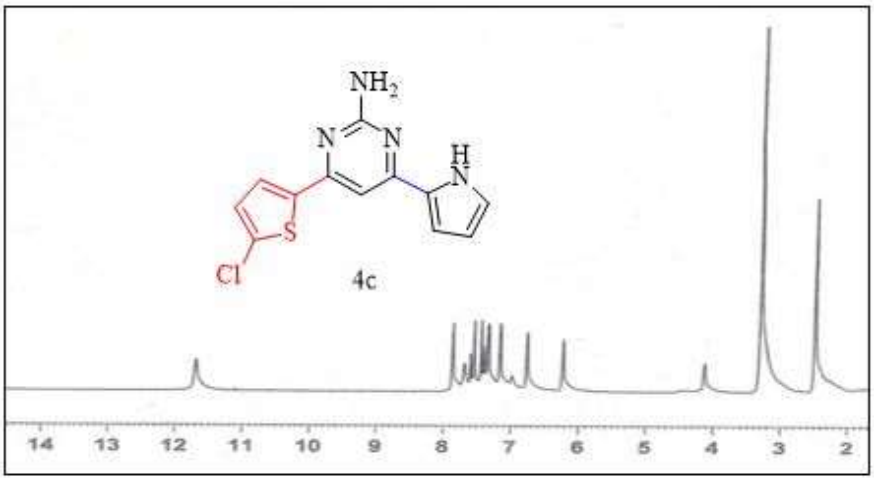

Figure 1. ^{1}HNMR (DMSO- *d6*) spectrum of compound **4c.**

3.2 Glyoxalase inhibitory Activity

In the present study, a series of synthesized pyrimidine derivatives were evaluated for their inhibitory effects on GLO-I enzyme. The results, summarized in Table 1, showed varying degrees of percent inhibition.

These findings provide insights into the structure-activity relationships (SARs) of these compounds and their potential as glyoxalase I inhibitors (Figure 2). Compound **5b** demonstrated the greatest inhibition (90%), with an IC_{50} value of 15 µM, indicating potent inhibitory activity. The presence of a dichloro-thiophene ring (as in **5a-c**) seems to enhance the glyoxalase inhibitory activity compared to the simpler chloro-thiophene ring (as in **4a-d**). However, the presence of a furan ring substituent in **5b** improved the activity compared to thiophene and pyrrole substituent on the pyrimidine scaffold. The observed SAR implies that the electronic and steric properties imparted by the substituents on the pyrimidine ring are crucial for the enzyme inhibitory activity. The results presented in this study align with prior research, suggesting that the presence of a chlorine at the para position of the benzene ring enhances the inhibitory activity of GLO-I [9, 42]. This enhancement can be attributed to the electron-withdrawing effect of the chlorine atom and the favourable steric interactions occurring at the active site of GLO-I.

These results highlight the importance of chlorine atoms as well as furan heterocycle in enhancing the inhibitory activity against the glyoxalase enzyme. The variation in inhibition percentages suggested structure-dependent activity, providing valuable insights for the future design and synthesis of more potent glyoxalase inhibitors.

Table 1. Glyoxalase I inhibitory activity of synthesized compounds.

Compound number	Percent of inhibition
4a	21.0%
4b	NA [1]
4c	27.0%
4d	41.3%
5a	67.0%
5b [2]	90.0% (IC_{50}= 15 µM)***
5c	53.0%

[1] NA: Not applicable
[2] IC_{50} values were calculated for compounds showing >75% inhibition.
*** P<0.0001. Statistical significance was determined using one-way ANOVA for multiple comparisons.

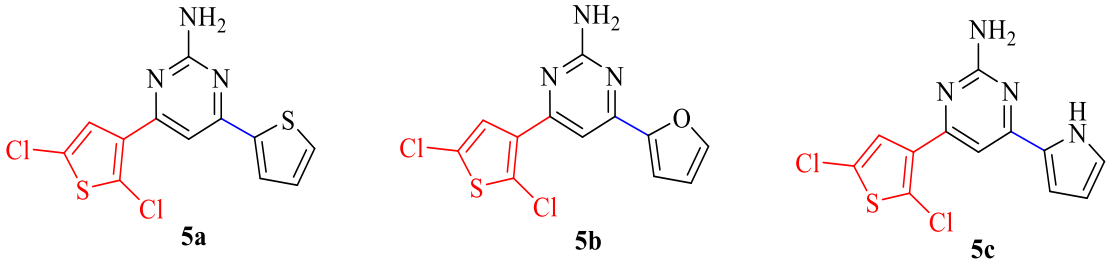

Figure 2. Chemical structures of the compounds with the highest inhibitory activity against GLO-I.

3.3. Molecular Docking Analysis

Molecular docking is a cornerstone computational technique in the field of drug discovery, offering valuable insights into the interaction dynamics and binding affinities between ligands and their respective receptors [43-46]. This technique is instrumental in simulating the formation of complexes between small molecules and macromolecular targets, thereby facilitating the prediction of ligand orientation within binding sites—a key factor in understanding the specificity and efficacy of molecular interactions [43-46]. As a computational approach, it is integral to rational drug design, enabling researchers to efficiently screen a multitude of compounds and identify those with the most promising therapeutic profiles [43-46].

This study employed molecular docking analysis using AutoDock 4.2 to elucidate the interaction mechanism of synthesized compounds, which was attributed to their GLO-I inhibitory activity compared to that of the cocrystallized ligand. The present simulation focused on those exhibiting the highest *in vitro* inhibitory activity against glyoxalase I, specifically compounds **5a-c** [47].

To validate the docking procedure, the cocrystallized ligand *N*-hydroxypyridone (control) was extracted from the crystal structure (PDB code: 3VW9) [23] and redocked into the same active binding site of the enzyme using AutoDock 4.2 (Figure 3). The results demonstrated that the method was capable of placing the control in a similar conformation to its crystal structure, with a root mean square deviation (RMSD) of approximately 0.61 Å and a binding affinity of approximately -10.62 kcal/mol (Table 2). The RMSD was within the acceptable range for computational docking studies [26-31, 48].

Figure 3 displays various types of interactions, such as hydrogen bonds, metal-acceptor interactions, and hydrophobic contacts, which are essential for stabilizing the ligand in the enzyme's binding pocket. Coordination with a zinc (Zn) atom is fundamental to these interactions and is crucial for enzyme activity [23]. Additionally, the hydrogen bonds formed with the amino acids GLU99, GLN33, and HIS126 play a key role in orienting the ligand for effective Zn interactions. Hydrophobic interactions, including π-alkyl and π-sigma interactions with target residues such as LEU160 and PHE162, also contribute significantly to binding specificity and energetics. This suggests that AutoDock 4.2 was successful in reproducing the cocrystallized structure with crucial interactions, and the same parameters can be used to dock the synthesized compounds with the enzyme.

Table 2 and Figure 4 provide an extensive overview of the binding affinities (ΔG_{bind} in kcal/mol) and the molecular interactions of **5a**, **5b**, and **5c**, as well as the cocrystallized ligand (N-hydroxypyridone), within the active binding site of human glyoxalase I (PDB ID: 3VW9). It is clear from Figure 3 that none of the docked compounds (**5a-c**) directly interact with the zinc (Zn) atom within the active site of GLO-I. The absence of direct metal-acceptor interactions with Zn for these compounds contrasts with the cocrystallized ligand, which is engaged in such interactions, as previously analysed in Figure 3.

Compound **5a** is primarily stabilized by hydrophobic interactions with MET 65, MET179, MET183, HIS126 and LEU182. Despite these contacts, the absence of direct coordination to the Zn atom and a less diversified interaction profile may account for its relatively lower free binding energy of -6.65 kcal/mol. On the other hand, **5b** exhibits a favourable binding affinity of -8.38 kcal/mol and displays several hydrophobic interactions, in addition to multiple hydrogen bonds involving the GLU172 and HIS126 residues. This distinctive interaction profile among the docked compounds could elucidate its potent *in vitro* inhibitory activity. Similarly, compound **5c** showed a network of hydrophobic interactions and a single hydrogen bond with GLU99, resulting in a docking score of -7.99 kcal/mol.

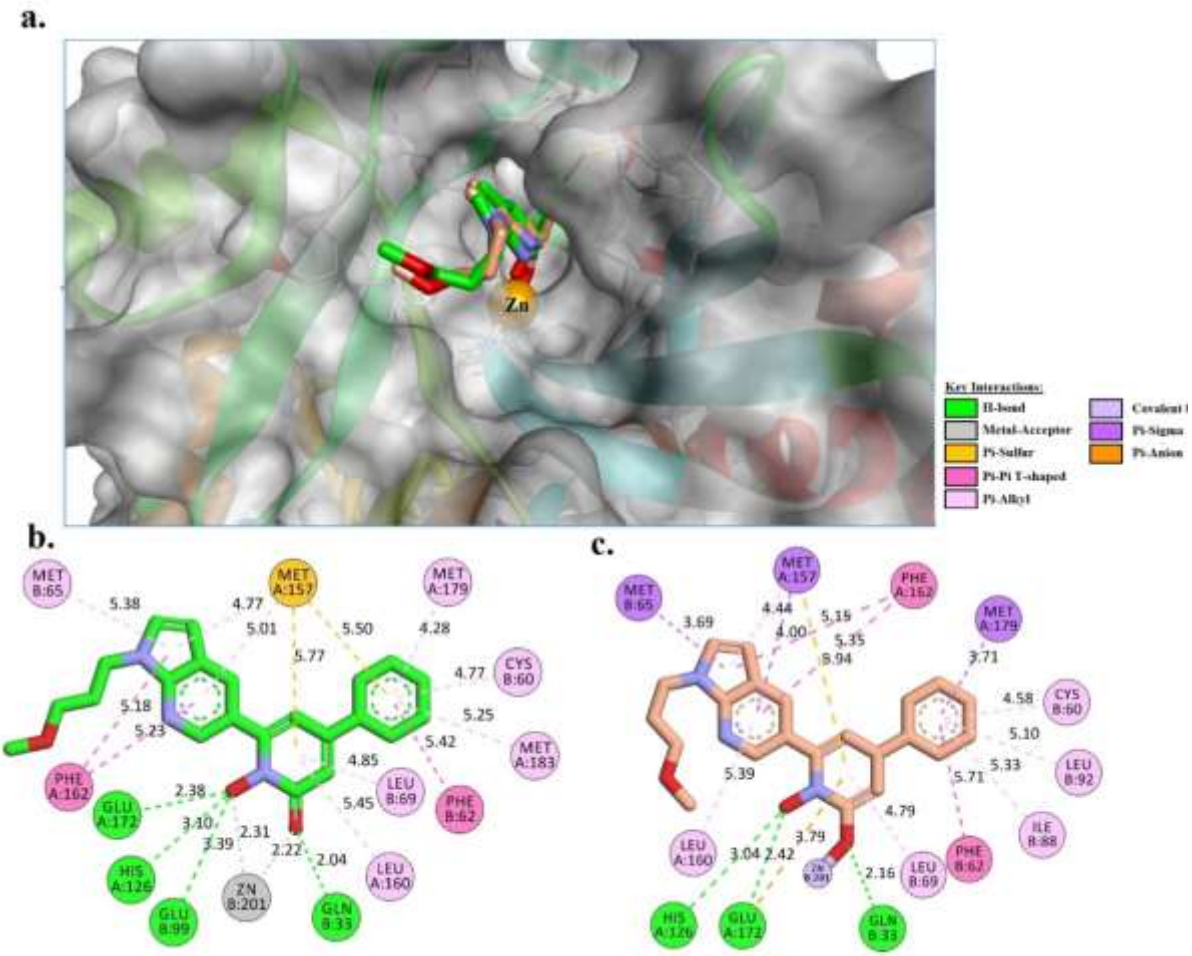

Figure 3. (**a**) Superimposition and (**b**) 2D interaction analysis of the original binding pose of the cocrystallized ligand, *N*-hydroxypyridone (represented in green for carbon (C), red for oxygen (O), and navy for nitrogen (N)). (**c**) Redocked Ligand (shown in pale pink (salmon) for carbon (C), red for oxygen (O), and navy for nitrogen (N)) within the active binding site of the crystal structure of Human Glyoxalase I (GLO1) (PDB ID: 3VW9). The root-mean-square deviation (RMSD) between the original and redocked binding poses was found to be 0.61 Å.

Table 2. Docking scores (ΔG_{bind} in kcal/mol) of the of **5a**, **5b**, and **5c**, as well as the cocrystallized ligand (*N*-hydroxypyridone), within the active binding site of the Human Glyoxalase I (PDB ID: 3VW9), assessed using AutoDock 4.2.

Compound number	**ΔG_{bind} (kcal/mol)**
5a	-6.65
5b	-8.38
5c	-7.99
Cocrystalized ligand	-10.62

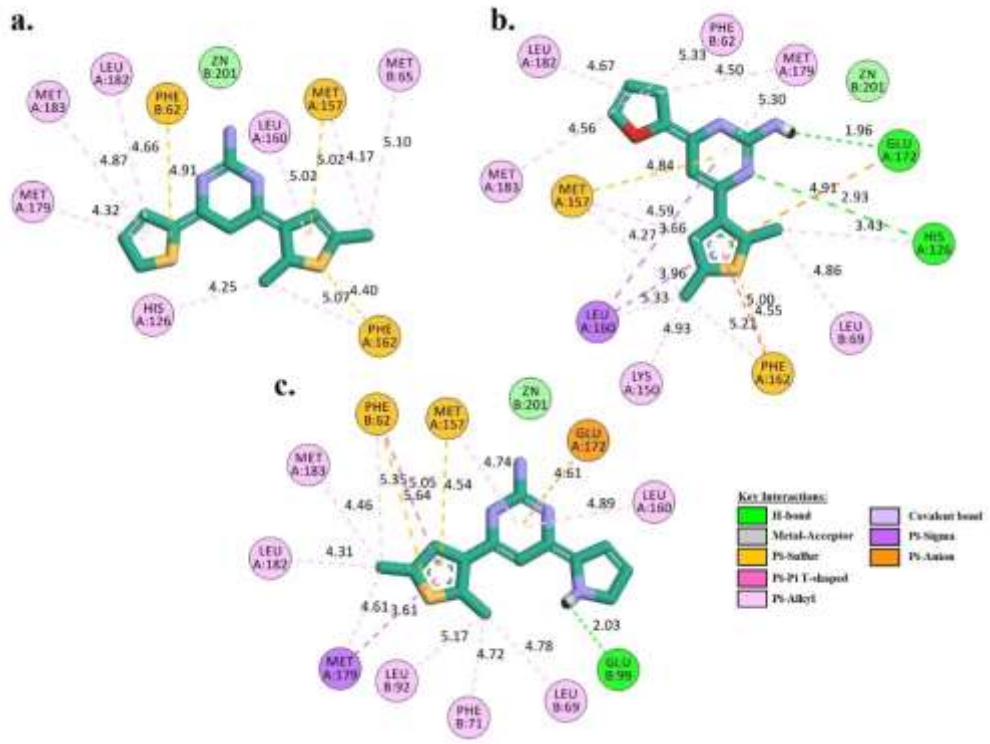

Figure 4. 2D molecular interactions models of the of the of **5a** (**a**), **5b** (**b**), and **5c** (**c**) within the active binding site of the Human Glyoxalase I (GLO-I).

The docking scores from Table 2, especially the highest binding affinity observed for the cocrystallized ligand at -10.62 kcal/mol, indicate that direct interactions with Zn are likely a significant contributor to binding strength. The lack of such interactions in the studied compounds underscores the necessity for further structural refinement to introduce functionalities that can engage directly with the Zn atom in the binding site. Hence, future investigations should prioritize the enhancement of metal-binding properties in designing GLO-I inhibitors, potentially through the inclusion of chelating groups that could facilitate such interactions. This strategy may lead to improved binding affinities and could result in inhibitors that more closely mimic the action of the cocrystallized ligand. The exploration of these structural modifications will be essential for the development of more potent GLO-I inhibitors.

4. Conclusions

A new series of pyrimidine-2-amine derivatives were successfully synthesized in good to very good yields. All new compounds were characterized by standard spectroscopic techniques. *In vitro* assays demonstrated that pyrimidine derivatives, particularly **5b**, exhibit significant inhibitory activity against GLO-I, with an IC_{50} value of 15 µM. Molecular docking analysis using AutoDock 4.2 further elucidated the interaction mechanisms of these compounds within the GLO-I active site. *In vitro* and *in silico* findings contribute to the understanding of the structure-activity relationships governing enzyme inhibition and pave the way for the rational design of more potent and selective GLO-I inhibitors. The presence of dichloro-thiophene and furan ring substituents significantly enhanced the inhibitory activity, highlighting the importance of structural modifications of the pyrimidine scaffold in achieving effective enzyme inhibition. Moreover, the absence of direct metal-acceptor interactions with the zinc atom in the active site of GLO-I for the studied compounds suggests an area for further structural refinement. Introducing functionalities capable of engaging directly with the zinc atom could enhance binding affinities and mimic the action of more potent inhibitors.

In summary, this research not only advances our understanding of the glyoxalase system and its role in disease pathogenesis but also provides a foundational framework for the development of new therapeutic agents. The insights gained from this study are expected to have significant implications in the field of drug discovery, especially in designing targeted therapies for diseases associated with glyoxalase dysregulation.

Author Contributions: Conceptualization, M.I.; methodology, M.M.A., E.M. and Q.B.; software, M.B.A.; validation, M.M.A.; formal analysis, M.I. and M.R.; investigation, M.I.; writing—original draft preparation, M.I.; writing—review and editing, M.I., M.M.A., E.M. and M.B.A.; supervision, M.I. All authors have read and agreed to the published version of the manuscript.

ACKNOWLEDGEMENTS"
Authors are grateful to Al Al-Bayt University (Mafraq, Jordan) and Jadara University (Irbid, Jordan).

Disclosure statement
The authors declare no conflicts of interest.

Funding:
This research was funded by Al al-Bayt University.

References:

1. Schalkwijk, C. and C. Stehouwer, *Methylglyoxal, a highly reactive dicarbonyl compound, in diabetes, its vascular complications, and other age-related diseases.* Physiol. Rev., 2020. **100**(1): p. 407-461.
2. Rabbani, N., M. Xue, and Paul J. Thornalley, *Activity, regulation, copy number and function in the glyoxalase system.* Biochemical Society Transactions, 2014. **42**(2): p. 419-424.
3. Allaman, I., M. Bélanger, and P.J. Magistretti, *Methylglyoxal, the dark side of glycolysis.* Front. Neurosci., 2015. **9**: p. 23.
4. Saeed, M., et al., *The role of glyoxalase in glycation and carbonyl stress induced metabolic disorders.* Curr. Protein Pept. Sci., 2020. **21**(9): p. 846-859.
5. Rabbani, N., M. Xue, and P.J. Thornalley, *Methylglyoxal-induced dicarbonyl stress in aging and disease: first steps towards glyoxalase 1-based treatments.* Clinical science, 2016. **130**(19): p. 1677-1696.
6. Kim, J.-Y., et al., *Glyoxalase 1 as a therapeutic target in cancer and cancer stem cells.* Molecules and cells, 2022. **45**(12): p. 869-876.
7. Al-Balas, Q.A., et al., *Identification of the First "Two Digit Nano-molar" Inhibitors of the Human Glyoxalase-I Enzyme as Potential Anticancer Agents.* Medicinal Chemistry, 2022. **18**(4): p. 473-483.
8. Al-Oudat, B.A., et al., *Design, synthesis and biological evaluation of novel glyoxalase I inhibitors possessing diazenylbenzenesulfonamide moiety as potential anticancer agents.* Bioorganic & Medicinal Chemistry, 2020. **28**(16): p. 115608.
9. Al-Balas, Q., et al., *Design, synthesis and biological evaluation of potential novel zinc binders targeting human glyoxalase-I; A validated target for cancer treatment.* Jordan Journal of Pharmaceutical Sciences, 2018. **11**(1).
10. Takasawa, R., et al., *Structure–activity relationship of human GLO I inhibitory natural flavonoids and their growth inhibitory effects.* Bioorganic & medicinal chemistry, 2008. **16**(7): p. 3969-3975.
11. Mahapatra, A., T. Prasad, and T. Sharma, *Pyrimidine: a review on anticancer activity with key emphasis on SAR.* Future J. Pharm. Sci., 2021. **7**(1): p. 123.
12. Ajani, O.O., et al., *Exploration of the chemistry and biological properties of pyrimidine as a privilege pharmacophore in therapeutics.* Int. J. Biol. Chem, 2015. **9**(4): p. 148-177.
13. Kreycy, N., et al., *Glyoxalase 1 expression is associated with an unfavorable prognosis of oropharyngeal squamous cell carcinoma.* BMC cancer, 2017. **17**(1): p. 1-9.
14. Shah, U., et al., *In Vitro Cytotoxicity and Aromatase Inhibitory Activity of Flavonoids: Synthesis, Molecular Docking and In Silico ADME Prediction.* Anti-Cancer Agents in Medicinal Chemistry (Formerly Current Medicinal Chemistry-Anti-Cancer Agents), 2022. **22**(7): p. 1370-1385.
15. El-Azim, A., et al., *Heterocyclization of Poly functionalized Pyrimidine: Novel Synthesis and Antiproliferative Evaluation of Azino and Azolo Pyrimidines.* Egyptian Journal of Chemistry, 2023. **66**(1): p. 239-248.
16. Zhou, Y., et al., *Discovery of selective 2, 4-diaminopyrimidine-based photoaffinity probes for glyoxalase I.* MedChemComm, 2014. **5**(3): p. 352-357.
17. Al-Maqtari, H., *Synthesis of Some New 4,6-(diheteroaromatic)-3-carbonitrile-2-oxo-1,2-didyropyridine Derivatives*. 2011, Al al-Bayt University: Jordan.
18. Patel, A., et al., *Synthesis of new flavanoid and chalcone derivatives as antimicrobial agent by green chemistry approach.* International Journal of Pharmaceutical Sciences and Research, 2017. **8**(6): p. 2725-2730.
19. Aladamat, M., *Synthesis and biological activity of new 4,6-(diheteroaromatic)pyrimidine-2-amines*. 2014, Al al-Bayt University: Jordan.
20. Mukhtar, S.S., et al., *A review of chalcones: synthesis, reactions, and biological importance.* Egyptian Journal of Chemistry, 2022. **65**(8): p. 379-395.
21. Al-Balas, Q.A., et al., *Computational and experimental exploration of the structure–activity relationships of flavonoids as potent glyoxalase-I inhibitors.* Drug Development Research, 2018. **79**(2): p. 58-69.
22. Al-Shar'i, N.A., et al., *Ellagic acid: A potent glyoxalase-I inhibitor with a unique scaffold.* Acta Pharmaceutica, 2021. **71**(1): p. 115-130.
23. Chiba, T., et al., *Design and evaluation of azaindole-substituted N-hydroxypyridones as glyoxalase I inhibitors.* Bioorganic & medicinal chemistry letters, 2012. **22**(24): p. 7486-7489.
24. Westbrook, J., et al., *The protein data bank and structural genomics.* Nucleic acids research, 2003. **31**(1): p. 489-491.
25. Biovia, D.S., *Discovery studio visualizer.* San Diego, CA, USA, 2017. **936**.
26. Al-Thiabat, et al., *Conjugated β-cyclodextrin enhances the affinity of folic acid towards FRα: molecular dynamics study.* Molecules, 2021. **26**(17): p. 5304.
27. Amir Rawa, M.S., et al., *Naturally Occurring 8ß, 13ß-kaur-15-en-17-al and Anti-Malarial Activity from Podocarpus polystachyus Leaves.* Pharmaceuticals, 2022. **15**(7): p. 902.

28. Larue, L., et al., *tLyp–1: A peptide suitable to target NRP–1 receptor.* Bioorg. Chem., 2023. **130**: p. 106200.
29. Alidmat, M.M., et al., *Synthesis, Characterization, Molecular Docking and Cytotoxicity Evaluation of New Thienyl Chalcone Derivatives against Breast Cancer Cells.* Sys Rev Pharm., 2022. **13**(1).
30. Al-Thiabat, et al., *Heterocyclic substitutions greatly improve affinity and stability of folic acid towards FRα. An in silico insight.* Molecules, 2021. **26**(4): p. 1079.
31. Alhawarri, M., et al., *Potential Anti-Cholinesterase Activity of Bioactive Compounds Extracted from Cassia grandis Lf and Cassia timoriensis DC.* . Plants, 2023.
32. Alhawarri, M.B., et al., *ADME profiling, molecular docking, DFT, and MEP analysis reveal cissamaline, cissamanine, and cissamdine from Cissampelos capensis Lf as potential anti-Alzheimer's agents.* RSC advances, 2024. **14**(14): p. 9878-9891.
33. Dolinsky, T.J., et al., *PDB2PQR: expanding and upgrading automated preparation of biomolecular structures for molecular simulations.* Nucleic acids research, 2007. **35**(2): p. 522-525.
34. Olsson, M.H., et al., *PROPKA3: consistent treatment of internal and surface residues in empirical pKa predictions.* Journal of chemical theory and computation, 2011. **7**(2): p. 525-537.
35. Williams, C.J., et al., *MolProbity: More and better reference data for improved all-atom structure validation.* Protein Science, 2018. **27**(1): p. 293-315.
36. Lanig, H., *8.2 Molecular Mechanics.* Chemoinformatics: Basic Concepts and Methods, 2018: p. 279.
37. Morris, G.M., et al., *AutoDock4 and AutoDockTools4: Automated docking with selective receptor flexibility.* Journal of computational chemistry, 2009. **30**(16): p. 2785-2791.
38. Xie, Y., et al., *Enhanced enzyme kinetic stability by increasing rigidity within the active site.* Journal of Biological Chemistry, 2014. **289**(11): p. 7994-8006.
39. Yunos, N.M., M.G. Al-Thiabat, and N.J. Sallehudin, *Quassinoids from Eurycoma longifolia as Potential Dihydrofolate Reductase Inhibitors: A Computational Study.* Current Pharmaceutical Biotechnology, 2024.
40. Fuhrmann, J., et al., *A new Lamarckian genetic algorithm for flexible ligand-receptor docking.* Journal of computational chemistry, 2010. **31**(9): p. 1911-1918.
41. Hill, A.D. and P.J. Reilly, *Scoring functions for AutoDock.* Glycoinformatics, 2015. **4**: p. 467-474.
42. Al-Balas, Q.A., et al., *Novel glyoxalase-I inhibitors possessing a "zinc-binding feature" as potential anticancer agents.* Drug design, development and therapy, 2016: p. 2623-2629.
43. De Ruyck, J., et al., *Molecular docking as a popular tool in drug design, an in silico travel.* Adv Appl Bioinforma Chem, 2016: p. 1-11.
44. Ferreira, L.G., et al., *Molecular docking and structure-based drug design strategies.* Molecules, 2015. **20**(7): p. 13384-13421.
45. Ma, D.-L., D.S.-H. Chan, and C.-H. Leung, *Molecular docking for virtual screening of natural product databases.* Chem. Sci., 2011. **2**(9): p. 1656-1665.
46. Meng, X.-Y., et al., *Molecular docking: a powerful approach for structure-based drug discovery.* Curr Comput Aided Drug Des., 2011. **7**(2): p. 146-157.
47. Norgan, A.P., et al., *Multilevel parallelization of AutoDock 4.2.* J. Cheminformatics, 2011. **3**: p. 1-9.
48. Yunos, N.M., et al., *In Vitro and In Silico Analysis of the Anticancer Effects of Eurycomanone and Eurycomalactone from Eurycoma longifolia.* Plants, 2023. **12**(15): p. 2827.